SI

Face-controlled chirality induction in octahedral thiacalixarene-based porous coordination cages

Ivan V. Khariushin,[a] Alexander S. Ovsyannikov,[b] Stéphane A. Baudron,[a] Jas S. Ward,[c] Anniina Kiesila¨,[c] Kari Rissanen,[c] Elina Kalenius,[c] Matthieu Chessé,[d] Beata Nowicka,[e] Svetlana E. Solovieva,[f] Igor S. Antipin,[f] Véronique Bulach[a] and Sylvie Ferlay*[a]

[a] Université de Strasbourg, CNRS, CMC UMR 7140, F-67000 Strasbourg, FRANCE. E-mail: ferlay@unistra.fr
[b] Arbuzov Institute of Organic and Physical Chemistry, FRC Kazan Scientific Center, Russian Academy of Sciences, Arbuzova 8, Kazan, RUSSIAN FEDERATION
[c] University of Jyvaskyla, Department of Chemistry, 40014 Jyväskylä, FINLAND
[d] LIMA UMR 7042, Université de Strasbourg et CNRS et UHA, European School of Chemistry, Polymers and Materials (ECPM), 25 Rue Becquerel, F-67087 Strasbourg, FRANCE
[e] Faculty of Chemistry, Jagiellonian University, Gronostajowa 2, 30-387 Kraków, POLAND
[f] Kazan Federal University, Kremlevskaya 18, Kazan 420008, RUSSIAN FEDERATION

Chiral HPLC for Λ-Co(HL)$_3$ and Δ-Co(HL)$_3$

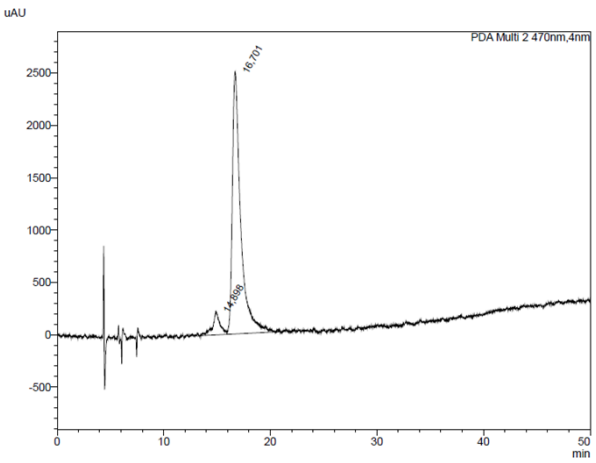

Λ-Co(HL)$_3$ (a)

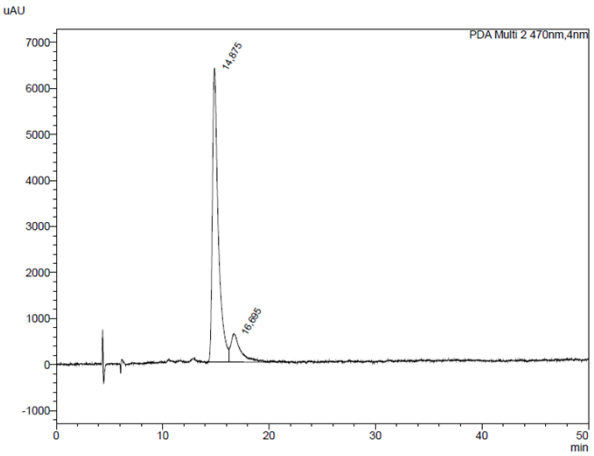

Δ-Co(HL)3 (b

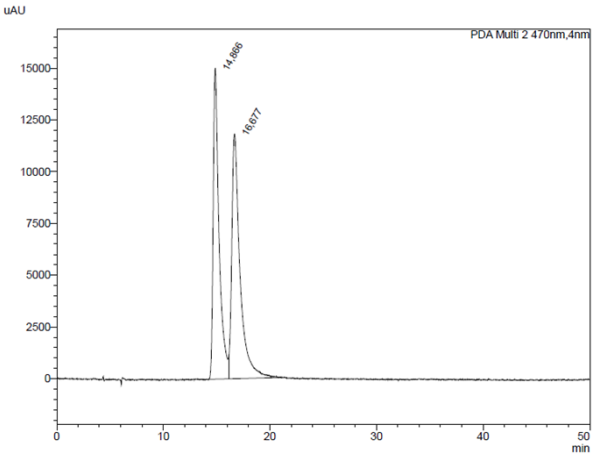

Racemic mixture (c)

Figure S1: HPLC chromatograms of a) **Λ-Co(HL)$_3$** b) **Δ-Co(HL)$_3$** and c) racemic mixture ***rac*-Co(HL)$_3$** for comparison

The asymmetric unit for the reported compounds

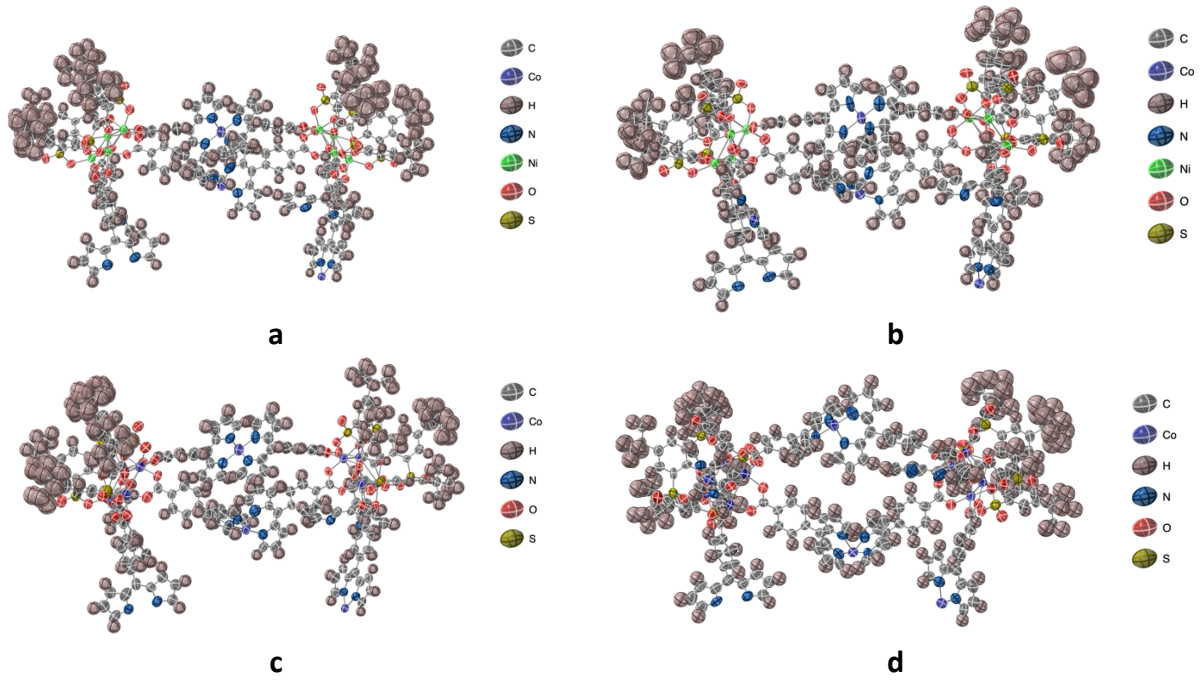

Figure S2: The asymmetric unit for a) **$[Ni_4SO_2TCA(\mu_4\text{-}OH_2)]_6[\Delta\text{-}Co(L)_3]_8 \bullet nDMF \bullet mH_2O$** b)) **$[Ni_4SO_2TCA(\mu_4\text{-}OH_2)]_6[\Lambda\text{-}Co(L)_3]_8 \bullet nDMF \bullet mH_2O$** c) **$Co_4SO_2TCA(\mu_4\text{-}OH_2)]_6[\Delta\text{-}Co(L)_3]_8 \bullet nDMF \bullet mH_2O$** and d) **$[Co_4SO_2TCA(\mu_4\text{-}OH_2)]_6[\Lambda\text{-}Co(L)_3]_8 \bullet nDMF \bullet mH_2O$** cages. Thermal ellipsoids are at 50% probability.

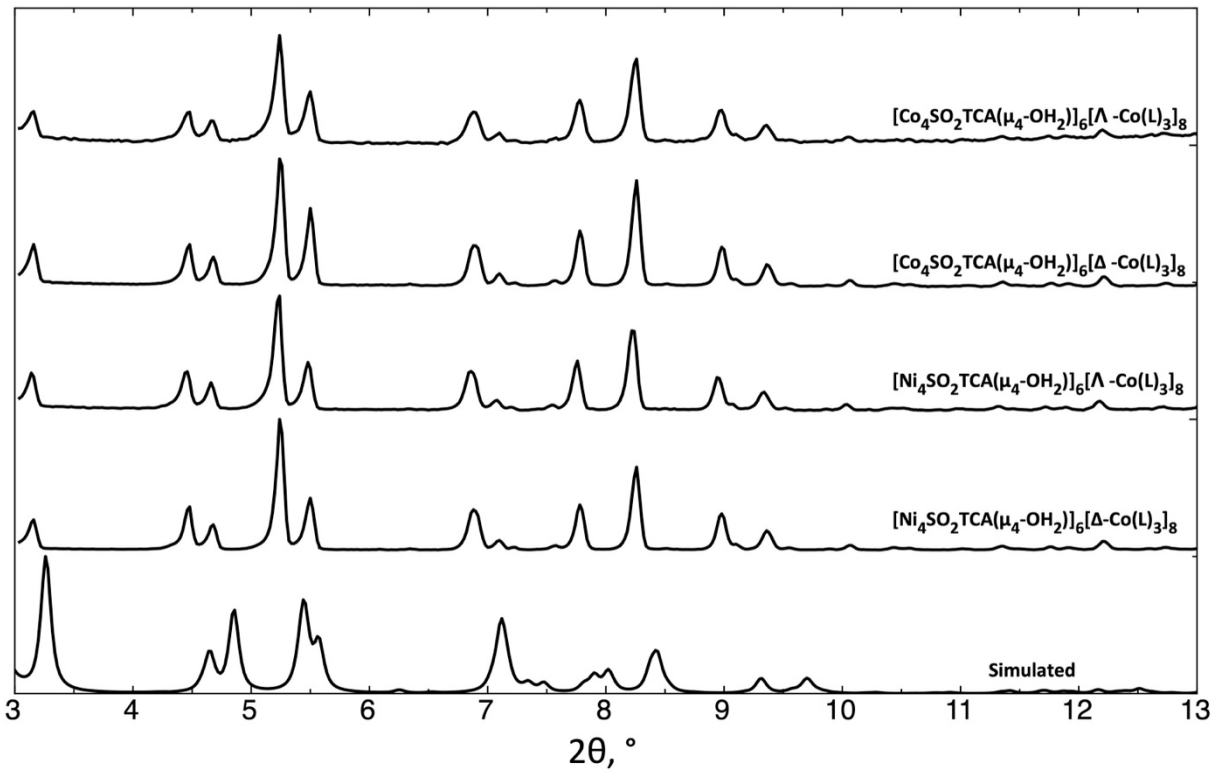

Figure S3. The powder X-Ray diffraction (PXRD) patterns for freshly prepared compounds in their mother liquor, **$[M_4SO_2TCA(\mu_4\text{-}OH_2)]_6[\Delta/\Lambda\text{-}Co(L)_3]$** (M = Ni or Co) compared to the simulated diagram for **$[Ni_4SO_2TCA(\mu_4\text{-}OH_2)]_6[\Lambda\text{-}Co(L)_3]_8$**

ESI-MS spectra

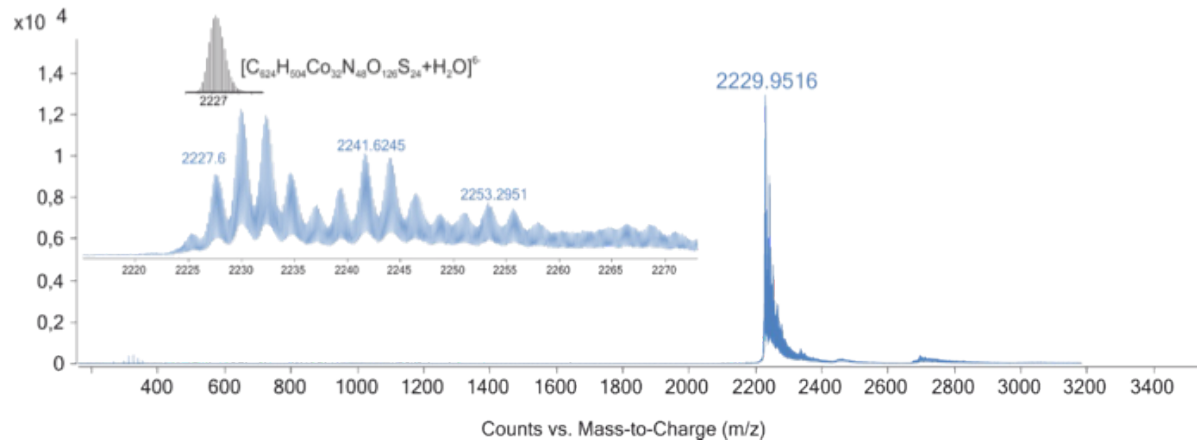

$[Co_4SO_2TCA(\mu_4\text{-}OH_2)]_6[\Delta\text{-}Co(L_1)_3]_8$

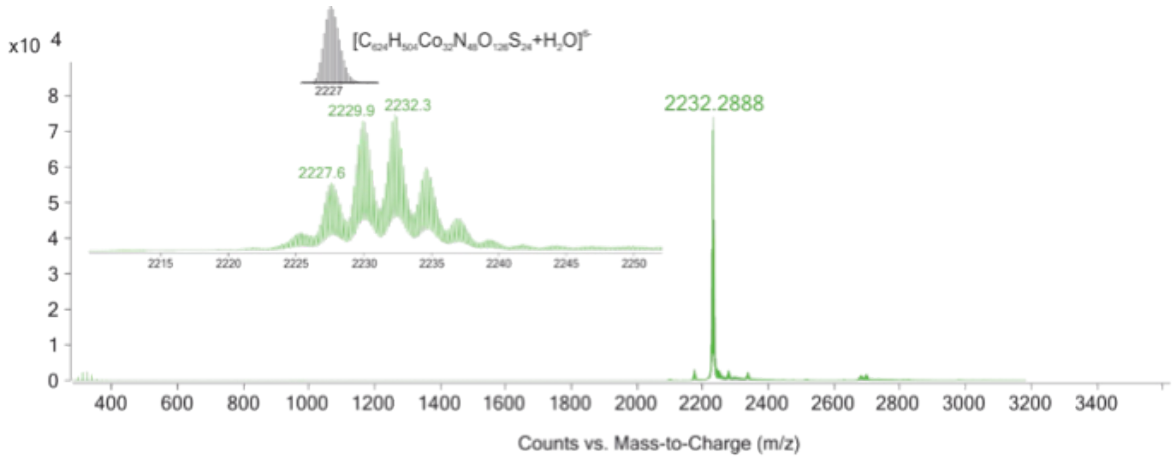

$[Co_4SO_2TCA(\mu_4\text{-}OH_2)]_6[\Lambda\text{-}Co(L_1)_3]_8$

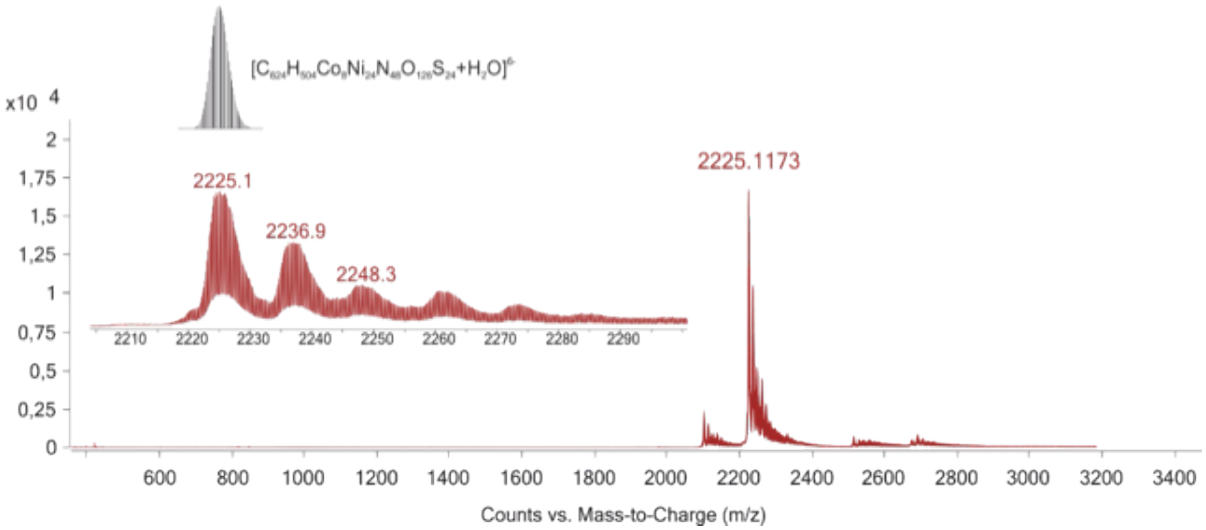

$[Ni_4SO_2TCA(\mu_4\text{-}OH_2)]_6[\Delta\text{-}Co(L_1)_3]_8$

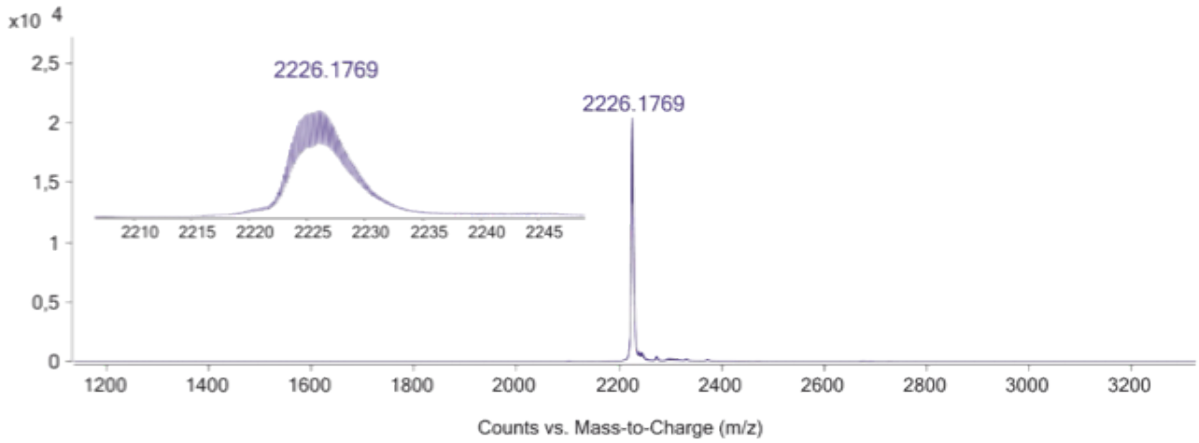

$[Ni_4SO_2TCA(\mu_4\text{-}OH_2)]_6[\Lambda\text{-}Co(L_1)_3]_8$

Figure S4 ESI-MS data for **$[M_4SO_2TCA(\mu_4\text{-}OH_2)]_6[\Lambda/\Delta\text{-}Co(L)_3]_8$** (M = Ni or Co) . Insets on left show zoomed view for base peak and peaks originating from different adducts. Comparison to theoretical isotopic pattern is given to H_2O adduct (ion at *m/z* 2227) with black line.

IM-MS calculations

The theoretical values of $^{T}CCS_{N2}$ can be calculated from the linear size of the obtained MOCs and the linear size of the buffer gas molecules (N_2). From the crystallographic data, it was possible to estimate the size of the cage, as a distance between two most remote methyl groups of the opposite shuttlecock moieties (diameter(cage) approximately 45.6Å), and Van der Waals radius of N_2 is approximately 1.55Å, which results in the following equation:

$$^{T}CCS_{N2} = \pi * (r(cage) + r(N_2))^2$$

$$^{T}CCS_{N2} = \pi * (22.8 + 1.55)^2 = \underline{1862.72\ Å^2}$$

	$^{DT}CCS_{N2}$
$[Co_4SO_2TCA(\mu_4\text{-}OH_2)]_6[\Lambda\text{-}Co(L_1)_3]_8$	1830.0
$[Co_4SO_2TCA(\mu_4\text{-}OH_2)]_6[\Delta\text{-}Co(L_1)_3]_8$	1833.6
$[Ni_4SO_2TCA(\mu_4\text{-}OH_2)]_6[\Lambda\text{-}Co(L_1)_3]_8$	Not resolved
$[Ni_4SO_2TCA(\mu_4\text{-}OH_2)]_6[\Delta\text{-}Co(L_1)_3]_8$	1846.1

Table S1: experimental $^{DT}CCS_{N2}$ for each MOC

CD spectra for $[Co_4SO_2TCA(\mu_4\text{-}OH_2)]_6[\Lambda/\Delta\text{-}Co(L)_3]_8$

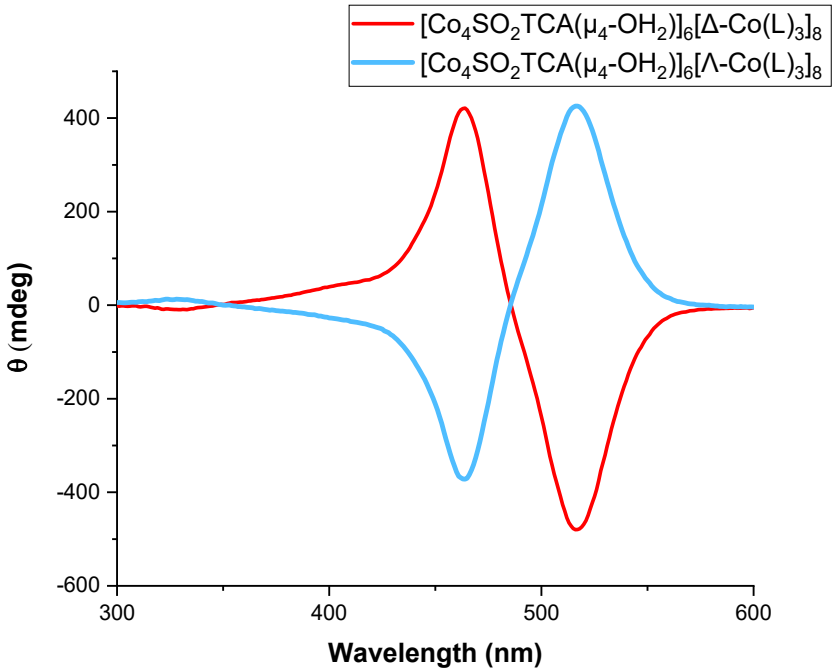

Figure S5: CD spectra for **$[Co_4SO_2TCA(\mu_4\text{-}OH_2)]_6[\Lambda/\Delta\text{-}Co(L)_3]_8$** (RT, $5*10^{-5}$M, THF, 2 mm)

Chiral HPLC for $[M_4SO_2TCA(\mu_4\text{-}OH_2)]_6[\Lambda/\Delta\text{-}Co(L)_3]_8$ (M = Ni or Co)

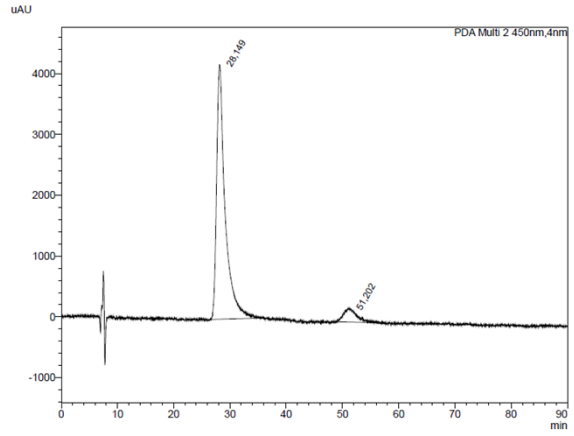

$[Ni_4SO_2TCA]_6[\Delta\text{-}Co(L)_3]_8$

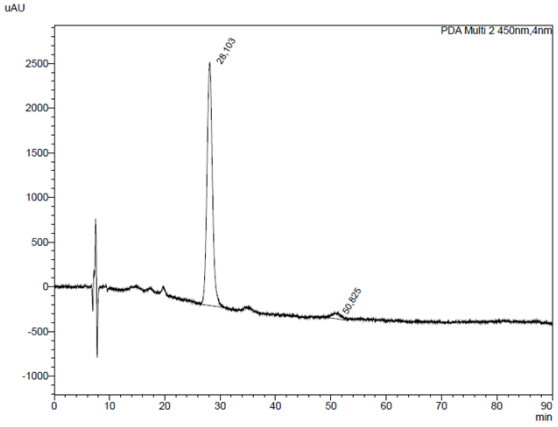

$[Co_4SO_2TCA]_6[\Delta\text{-}Co(L)_3]_8$

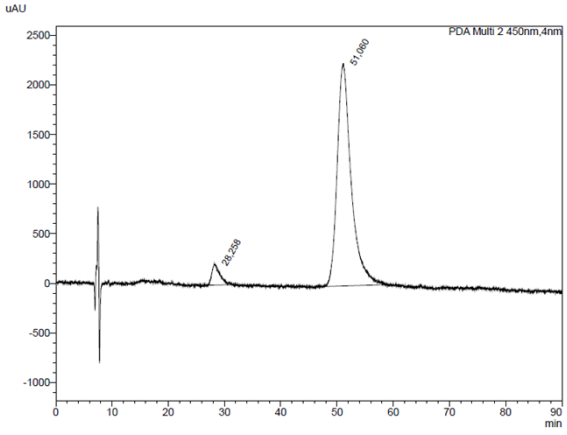

$[Ni_4SO_2TCA]_6[\Lambda\text{-}Co(L)_3]_8$

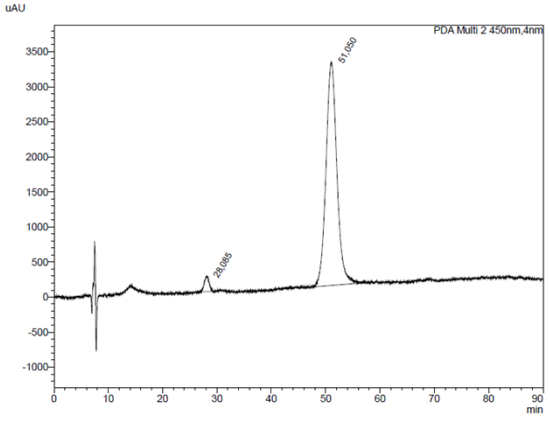

$[Co_4SO_2TCA]_6[\Lambda\text{-}Co(L)_3]_8$

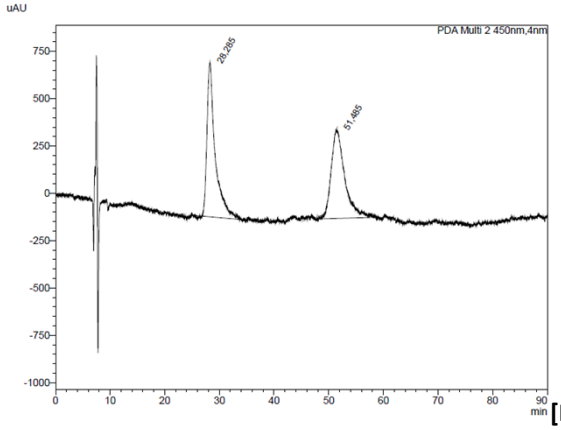

$[Ni_4SO_2TCA]_6[rac\text{-}Co(L)_3]_8$

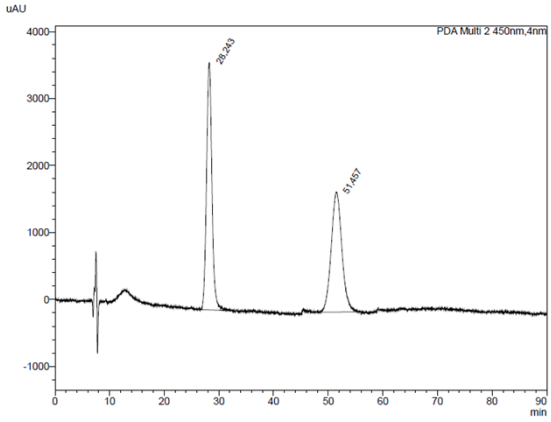

$[Co_4SO_2TCA]_6[rac\text{-}Co(L)_3]_8$

Figures S6: For comparison, HPLC chromatograms of $[M_4SO_2TCA(\mu_4\text{-}OH_2)]_6[\Lambda/\Delta\text{-}Co(L)_3]_8$ (M = Ni or Co) together with their racemic mixtures

Sorption properties of octahedral M_{32} cages

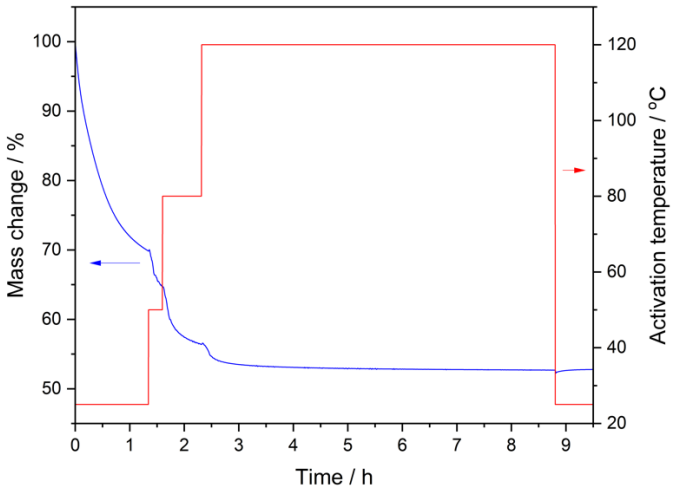

Figure S7: Temperature increase and mass loss upon stepwise activation of freshly filtered off **$[Co_4SO_2TCA(\mu_4\text{-}OH_2)]_6[\Lambda\text{-}Co(L)_3]_8$** sample.

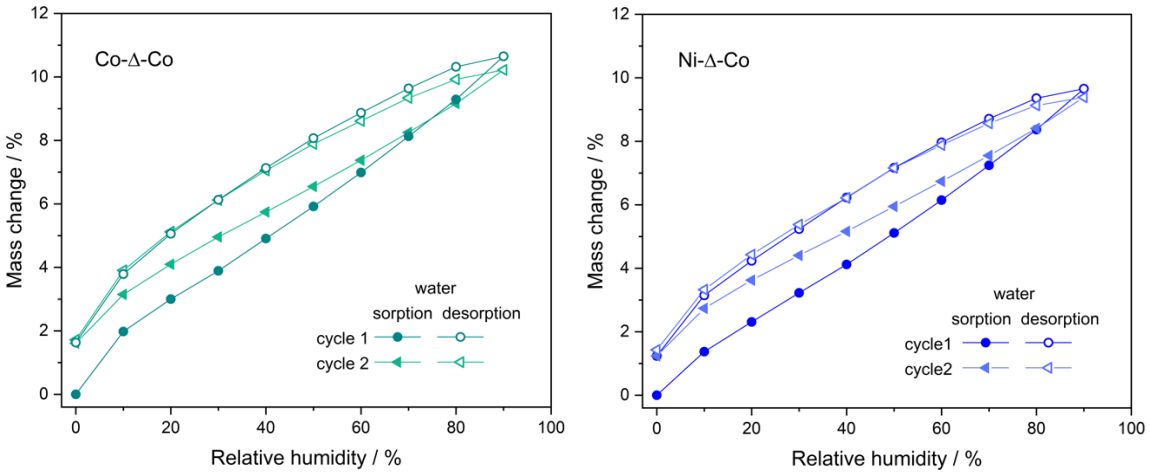

Figure S8: Isotherms of subsequent cycles of water sorption for **$[M_4SO_2TCA(\mu_4\text{-}OH_2)]_6[\Delta\text{-}Co(L)_3]_8$** (M = Ni or Co) showing retention of adsorbed of water, which can be removed in the re-activation process at 120°C.

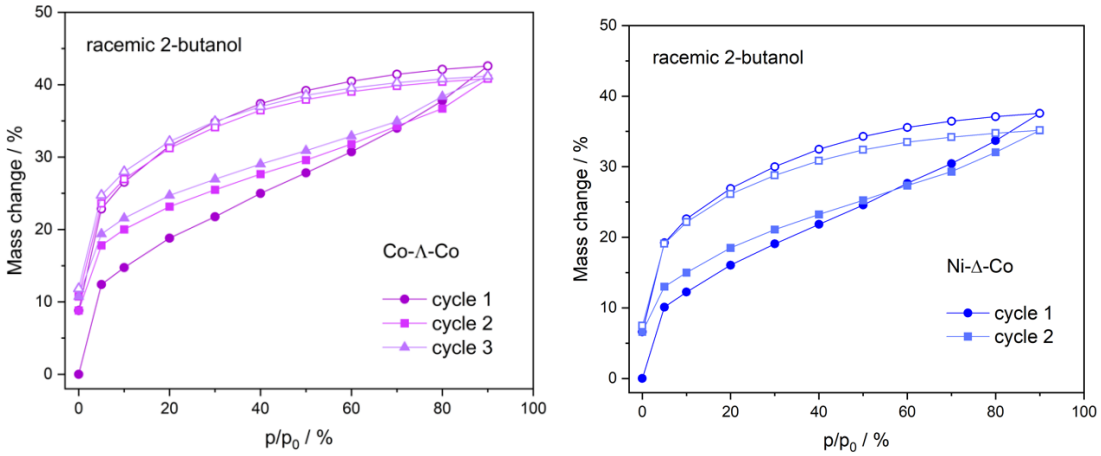

Figure S9: Isotherms of subsequent cycles of racemic 2-butanol sorption for **$[M_4SO_2TCA(\mu_4\text{-}OH_2)]_6[\Delta/\Lambda\text{-}Co(L)_3]_8$** (M = Ni or Co) showing retention of adsorbed of 2-butanol, which can be removed in the re-activation process at 120°C.

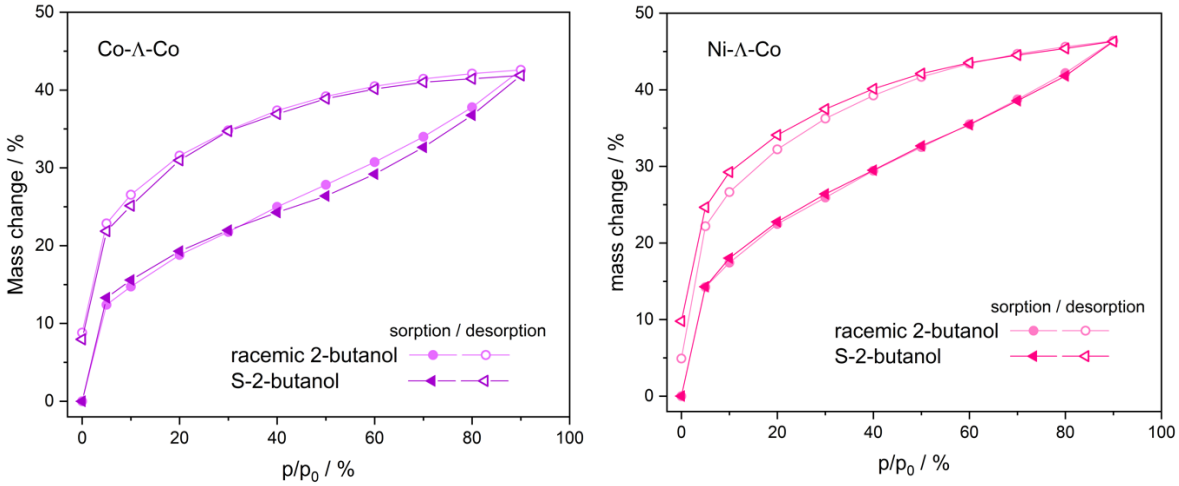

Figure S10: Comparison of sorption of racemic 2-butanol and enantiopure S-2-butanol for **$[M_4SO_2TCA(\mu_4\text{-}OH_2)]_6[\Lambda\text{-}Co(L)_3]_8$**.